Robotica: page 1 of 22. © Cambridge University Press 2017
doi:10.1017/S0263574717000200

Robust adaptive control of door opening by a mobile rescue manipulator based on unknown-force-related constraints estimation

Liang Ding†, Kerui Xia†,*, Haibo Gao†, Guangjun Liu‡ and Zongquan Deng†

†*State Key Laboratory of Robotics and System, Harbin Institute of Technology, Harbin, 150001, P. R. China. E-mails: liangding@hit.edu.cn, gaohaibo@hit.edu.cn, dengzq@hit.edu.cn*
‡*Department of Aerospace Engineering, Ryerson University, Toronto, Ontario, M5B 2K3, Canada. E-mail: gjliu@ryerson.ca*

(Accepted April 1, 2017)

SUMMARY
This study focuses on a door-opening mobile manipulator operating in four phases (reaching the door, grasping the door handle, turning the door handle, and pulling the door). We use force/torque feedback-based control, achieving compliance of the mobile base when it comes into contact with the handle. A method is proposed for estimating the unknown force-related constraints from manipulator joint position measurements. A robust adaptive control strategy is developed for tracking the planned trajectory to open the door. Finally, a mobile manipulator opens a real door with a locked latch and unknown force-related constraints, demonstrating the validity of the proposed approach.

KEYWORDS: Rescue task, Door-opening, Mobile manipulator, Unknown-force-related constraints estimation, Robust adaptive control

1. Introduction

Opening a door is a typical example of a rescue task. When humans wearing protective clothing approach a door in a rescue environment with unknown constraints (physical, geometrical, or force related), they follow subconscious routines developed through years of practice in order to address the unknown parameters. However, the extreme physical conditions (e.g., high temperature, high humidity, or radiation) of some rescue environments are harmful to human health, even when protective clothing is worn. Hence, mobile manipulators are expected to be used for rescue tasks instead of human workers. Performing the same tasks with mobile manipulators in such rescue environments is quite challenging. First, the extreme physical constraints may cause conventional force/torque sensors without protection to stop working. Therefore, estimating unknown-force-related constraints using force/torque sensors without considering the harm imposed by physical constraints may be difficult to achieve. Furthermore, when force/torque sensors are protected, their weight is greatly increased and precision is reduced. It is difficult and expensive for heavy force/torque sensors to be assembled in a multi-joint manipulator. Moreover, estimation error may then be large, leading to large internal forces. Excessive internal forces are undesirable because they may cause the task to fail or may even cause damage to the hardware. For the door-opening problem, one of the fundamental requirements for successfully opening a door using a mobile manipulator in a rescue environment is to estimate unknown force-related constraints using methods that work with extreme physical constraints and have small error.

Recently, many researchers have investigated the door-opening problem with specific programming tailored to the proposed constraint. Niemeyer and Slotine [24] proposed a control method for following

* Corresponding author. E-mail: keruixia@gmail.com

the trajectory of least resistance in order to solve the door-opening problem; this method does not require a kinematic model of the door but needs high-resolution joint velocity measurements. Nagatani and Yuta [21-23] presented a strategy for opening doors that uses an analytical description of the door handle trajectory. In their research, they applied the concept of action primitives to door opening. Each action primitive is equipped with an error adjustment mechanism to cope with the accumulated positioning error of the mobile base. Compliant control is used for relaxation of the end effector in successfully accomplishing the door-opening task. These approaches can be understood as applications of conventional compliance control schemes to the door-opening problem. It is noteworthy that they rely on the assumption that constraints such as the position and radius of the door are known.

Some researchers chose to explore new designs of compliant mechanisms that led to robotic systems dedicated to the door-opening task with unknown constraints. Kobayashi *et al*. [12] have been developing some rescue robots, called utility mobile robots for search (UMRS), with compliant joints. Liu developed a modular reconfigurable robot (MRR) with joint modules supporting multiple working modes, specifically active and passive working modes (2008, 2011). By carefully choosing when and which joint module should be switched between these two working modes in a door-opening process without the need for compliance control and with less sensory and computational complexity, the door-opening experiment on a door simulator with adjustable radius, handle height, and opening force is confirmed. Chung *et al*. [3] designed a multi-fingered robotic hand for use with an indoor service robot called Public Service Robot 1 (PSR1). Active sensing algorithms were proposed to reduce the effects of uncertainties in the environment. Fingertip tactile sensors were used for estimating contact force and contact position. The computed contact force was used to carry out compliance control of the door-opening process. Brooks *et al*. [2] developed a mobile manipulator system called CARDEA, which uses a SEGWAY robotic mobility platform (RMP) base mechanism for locomotion equipped with a 15-DOF robotic arm. The robotic arm was designed for an unstructured environment and consisted of a series of elastic actuators to analyze the responses of behavior-based methods and dexterous manipulation. Through virtual spring models, human-like compliance was obtained and results were experimentally verified. The work can be understood as a solution that uses specially designed, sophisticated mechanical hardware. However, these robots either are only capable of opening ajar doors that are not spring loaded, or are not designed for grasping and turning door handles.

Intelligent control architecture was also demonstrated in recent research. Petersson *et al*. [26] presented high-level control of a mobile manipulator by relaxing force control. They used visual tracking to estimate the parameters for opening the door.[25] They also employed an additional wrist force sensor and applied compliance control schemes. Waarsing *et al*. [29] proposed a behavior-based controller for door opening with a mobile manipulator. The key for realizing such a behavior-based controller is cooperation among the mobile manipulator subsystems, i.e., locomotion and manipulator control systems. Klingbeil *et al*. [11] developed a vision-based learning algorithm capable of opening various types of doors without prior knowledge of the doors. Kragic *et al*. [13] demonstrated visual servoing architecture for finding the door handle and estimating the door parameters. Kim *et al*. [10] developed a special mobile manipulator called Hombot for opening a door. Hombot was equipped with an anthropomorphic arm with a double active universal joint (DAUJ) to guarantee the compact size of the manipulator. Jamisola *et al*. [7] and Khatib *et al*. [9] considered a mobile manipulator system as a macro–micro manipulator and proposed effective dynamic behavior models on the basis of this concept. Li *et al*. [16] proposed a method whereby the mobile manipulator is first transformed into a reduced chained form, and then motion control with hybrid variable signals compensate for parametric uncertainties and suppress bounded disturbances. In other studies on mobile manipulation, coordinated motion planning was proposed considering stability and manipulation.[5] In addition, there have been studies on the stable motion control of a mobile manipulator under unknown-external-force application from the environment, and robust force/motion control strategies have been presented (Li, Ge, Adams, and Wijesoma 2008).[6,16] These studies assumed that all sensors can be used in the working environment[14,15].

A general framework was proposed for opening doors and drawers in unknown environments. Their framework can be divided into four parts: detecting and localizing the handle, operating the handle while learning the kinematics model, integrating the learned model into the robot's semantic map, and re-using the model for future encounters. The framework has been well tested on the PR2 platform, and the approach was successful in 51.9% of all 104 trails.

Our door-opening control scheme offers original contributions in relation to prior research. First, we use force/torque feedback-based control from the base-mounted six-axis force/torque sensor, achieving compliance of the mobile base when it comes into contact with the handle. Because of the force/torque feedback, the mobile base is floating on the x_0y_0 plane. Thus, in the grasping process, the mobile base will move slowly to achieve the pose adjust. Then, after the end effector has already firmly grasped the handle, the mobile base will remain stable. A method is proposed for estimating the unknown force-related constraints on the basis of manipulator joint position measurements instead of force/torque sensors, which may be expensive or affected by computational delays and physical conditions (e.g., temperature, humidity, or radiation). Third, a robust adaptive control strategy with a corresponding stability proof is used to track the planning trajectory to open a door automatically. Furthermore, the experimental demonstration is accomplished by pulling open a real-life door with the characteristics of a locked latch and unknown force-related constraints using a wheeled mobile manipulator.

The rest of this paper is organized as follows. In Section 2, after a brief introduction to the door-opening scenario, we address task analysis, which is necessary for the subsequent door opening method. In Section 3, an unknown-force-related constraints analysis and estimate scheme is explained, which plays a dominant role in rescue tasks. In Section 4, a robust adaptive control strategy with a corresponding stability proof is used to track the planned trajectory to open a door automatically. Finally, experimental results are discussed in Section 5, followed by some conclusions in Section 6.

2. Task Analysis

For the door-opening task, the decision on how and when a mobile manipulator should be working is critical because it determines, to a great extent, the success and efficiency of the door-opening control. In this section, we address the task analysis, which is necessary for the subsequent door-opening method. Figure 1 shows a description of the scenario for the door-opening process (searching for/reaching the door, grasping the door handle, turning the door handle, and pulling the door). The shape of a door handle is limited to a rectangular block. A brief explanation of each phase is as follows:

Phase (A): Searching for/reaching the door is accomplished by visual tele-operation. In this study, a joystick associated with a rough, supporting 3D visual display is used for navigation. By using visual tele-operation, we can navigate a mobile manipulator to the front of the door and optimize the initial pose of the robot to grasp the door handle.

The coordinates of the wheeled mobile base consist of the position (x_B, y_B, z_B) and the rotation ϑ_B. The angular velocities of the right front and left front wheels are defined as $\dot{\vartheta}_{Br}$ and $\dot{\vartheta}_{Bl}$, respectively. The mobile manipulator moves on flat ground, so the generalized coordinates of the wheeled mobile base $\boldsymbol{q}_{BG}$ under the G_0 coordinate system are written as

$$q_{BG} = \begin{bmatrix} x_B & y_B & \vartheta_B & \vartheta_{Br} & \vartheta_{Bl} \end{bmatrix}^T \tag{1}$$

The symbols r_B, b_B denote the radius of the front wheels and the half-width of the wheeled base, respectively. The kinematics model of the wheeled base is shown as

$$\begin{bmatrix} \dot{x}_B \\ \dot{y}_B \\ \dot{\vartheta}_B \\ \dot{\vartheta}_{Br} \\ \dot{\vartheta}_{Bl} \end{bmatrix} = \begin{bmatrix} \cos\vartheta_B & 0 \\ \sin\vartheta_B & 0 \\ 0 & 1 \\ \frac{1}{r_B} & \frac{b_B}{r_B} \\ \frac{1}{r_B} & -\frac{b_B}{r_B} \end{bmatrix} \begin{bmatrix} u_B \\ \omega_B \end{bmatrix} \tag{2}$$

u_B, ω_B are related to the angular velocities of the right and left wheel; $v_B = [\, \dot{\vartheta}_{Br} \quad \dot{\vartheta}_{Bl} \,]^T$

$$\begin{bmatrix} u_B \\ \omega_B \end{bmatrix} = \begin{bmatrix} \frac{r_B}{2} & \frac{r_B}{2} \\ \frac{r_B}{2b_B} & -\frac{r_B}{2b_B} \end{bmatrix} \begin{bmatrix} \dot{\vartheta}_{Br} \\ \dot{\vartheta}_{Bl} \end{bmatrix} \tag{3}$$

Table I. Geometric and inertial parameters for the mobile base.

Symbol	Description
G_o	Global coordinate system
G_{body}	Center of mass coordinate system of the mobile base
P_e	Local coordinate system of the gripper
x_{B}, y_{B}, z_{B}	Centroid position of the mobile base in G_o
ϑ_{B}	Rotation of the mobile base in G_{body}
$\dot{\vartheta}_{\text{Br}}$,$\dot{\vartheta}_{\text{Bl}}$	Angular velocities of the right front and left front wheels
r_{B}, b_{B}	Radius of the front wheels and the half-width of the wheeled base
u_{B}, ω_{B}	Linear velocity and angular velocity G_o
$\mathbf{S}_{\text{B}}(\mathbf{q}_{\text{B}})$	Mapping from G_{body} to G_o

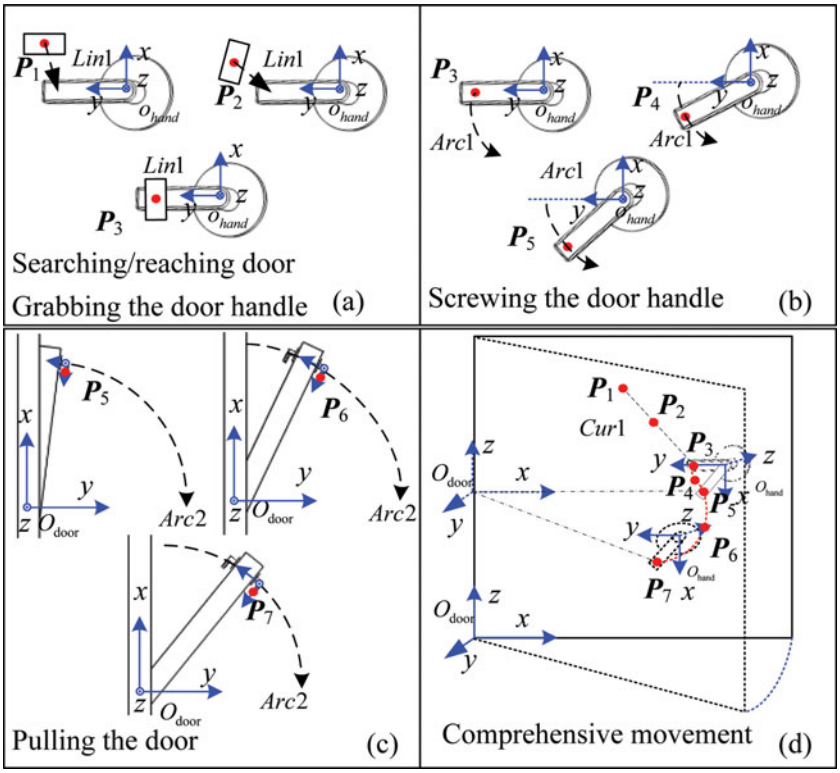

Fig. 1. Task analysis in door opening.

Thus, the kinematics model of the mobile base can be rewritten as

$$\dot{q}_{\text{B}} = S_{\text{B}}(q_{\text{B}})v_{\text{B}} \tag{4}$$

where

$$\dot{q}_{\text{B}} = [\,\dot{x}_{\text{B}} \quad \dot{y}_{\text{B}} \quad \dot{\vartheta}_{\text{B}}\,]^T,\ S_{\text{B}}(q_{\text{B}}) = \begin{bmatrix} \frac{r_{\text{B}}}{2}\cos\vartheta_{\text{B}} & \frac{r_{\text{B}}}{2}\cos\vartheta_{\text{B}} \\ \frac{r_{\text{B}}}{2}\sin\vartheta_{\text{B}} & \frac{r_{\text{B}}}{2}\sin\vartheta_{\text{B}} \\ \frac{r_{\text{B}}}{2b_{\text{B}}} & -\frac{r_{\text{B}}}{2b_{\text{B}}} \end{bmatrix}$$

The geometric parameters of the mobile base are summarized in Table I.

Phase (B): The mobile base is floating on the x_0y_0 plane. The manipulator realizes firm grasp of a door handle by tracking the trajectory represented by a straight line Lin1 as shown in Fig. 1(a). Indeed, a curve is better than a straight line in the grasping process. Thus, $\boldsymbol{P}_1$ is the initial position of the end effector, which is the optimized pose to grasp the door handle adjusted by tele-operation, and $\boldsymbol{P}_2$ is the grasping point, which is a known geometrical parameter or can be estimated. Meanwhile, the distance between the fingers of the end effector used in our study is larger than the distance between

Table II. Dependent parameters of the mobile base force/torque feedback control.

Symbol	Description
$\boldsymbol{P}_{\mathrm{i}}$	A series of positions under the O_{body} coordinate system
F_{base}	Force/torque from the base mounted six-axis force/torque sensor
δq_{B}	Incremental velocity of the wheeled mobile base
$\boldsymbol{K}_{\mathrm{base}}$	Mapping matrix from force/torque sensor to the wheel
C_{Function}	Output signal of the joystick

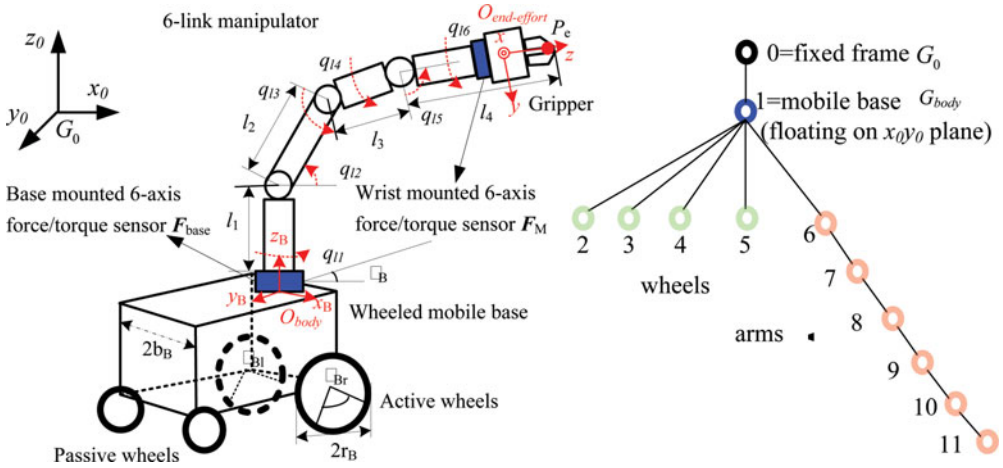

Fig. 2. Coordinates for the mobile manipulator.

the door handle and the door. Thus, a linear motion is used in the grasping process. The straight line Lin1 can be calculated by the interpolation method using point $\boldsymbol{P}_1$ $(x_1(t), y_1(t), z_1(t))$ and point $\boldsymbol{P}_2$ $(x_2(t), y_2(t), z_2(t))$ under the O_{body} coordinate system. It is noteworthy that visual depth information is inaccurate, so we use force/torque feedback from the base-mounted six-axis force/torque sensor as shown in Fig. 2, achieving compliance of the mobile base when it comes into contact with the handle. In this study, the mechanical decoupling of the mobile base and manipulator is realized by installing the force sensor between the manipulator and the mobile base.

Define the force/torque from the base mounted six-axis force/torque sensor as

$$F_{\mathrm{base}} = [\, f_{\mathrm{fx}} \quad f_{\mathrm{fy}} \quad f_{\mathrm{fz}} \quad n_{\mathrm{fx}} \quad n_{\mathrm{fy}} \quad n_{\mathrm{fz}} \,]^{\mathrm{T}} \tag{5}$$

where $f_{\mathrm{fx}}, f_{\mathrm{fy}}, f_{\mathrm{fz}}$ denote the sensor force from three directions, and $n_{\mathrm{fx}}, n_{\mathrm{fy}}, n_{\mathrm{fz}}$ denote the sensor torque from three directions.

The mapping of the sensor force/torque to the velocity of the wheeled mobile base can be given as

$$\delta q_{\mathrm{B}} = K_{\mathrm{base}} F_{\mathrm{base}} \tag{6}$$

The output signal of the joystick is defined as

$$C_{\mathrm{Function}} = \dot{q}_{\mathrm{B}} - \delta q_{\mathrm{B}} \tag{7}$$

From Eq. (7), one can see that the mobile base is floating on the $x_0 y_0$ plane when $\dot{q}_{\mathrm{B}}$=0. Thus, when the end-effector comes into contact with the handle, the mobile base will move slowly to achieve the pose adjust of the grasping process. The dependent parameters of the mobile base force/torque feedback control are summarized in Table II.

Phase (C): The mobile base remains stable. The manipulator realizes turning the door handle by tracking the trajectory represented by the arc Arc1 as shown in Fig. 1(b). The arc Arc1 can also be calculated by interpolation using points $\boldsymbol{P}_3$, $\boldsymbol{P}_4$, and $\boldsymbol{P}_5$. Above all, the points can be calculated by

the following formula, which is expressed as a function of the door handle's angle:

$$\theta_{\mathrm{h}} = \frac{\theta_{\mathrm{handle}}}{3} n,\ n = 1, 2, 3 \tag{8}$$

$$P_{3,4,5} = \begin{bmatrix} p_{\mathrm{x}} \\ p_{\mathrm{y}} \\ p_{\mathrm{z}} \end{bmatrix} = \begin{bmatrix} x_2 \\ r_{\mathrm{handle}}(1 - \cos\theta_{\mathrm{h}}) \\ z_2 - r_{\mathrm{handle}} \sin\theta_{\mathrm{h}} \end{bmatrix} \tag{9}$$

where r_{handle} denotes the rotation radius of the door handle; θ_{h} denotes the rotation angle of the door handle when reaching points $\boldsymbol{P}_3$, $\boldsymbol{P}_4$, and $\boldsymbol{P}_5$; and θ_{handle} denotes the rotation angle of the door handle when unlocked. It is noteworthy that points $\boldsymbol{P}_3$, $\boldsymbol{P}_4$, and $\boldsymbol{P}_5$ are calculated under the O_{hand} coordinate system; in the trajectory planning of door opening, these points must be converted to the O_{body} coordinate system.

Phase (D): The mobile base still remains stable. The manipulator realizes pulling the door by tracking the trajectory represented by the arc Arc2 as shown in Fig. 1(c). In addition, the interpolation points of arc Arc2 can be achieved by

$$\theta_{\mathrm{d}} = \frac{\theta_{\mathrm{door}}}{3} n,\ n = 1, 2, 3 \tag{10}$$

$$P_{5,6,7} = \begin{bmatrix} p_{\mathrm{x}} \\ p_{\mathrm{y}} \\ p_{\mathrm{z}} \end{bmatrix} = \begin{bmatrix} r_{\mathrm{door}}(1 - \cos\theta_{\mathrm{d}}) \\ y_5 - r_{\mathrm{door}} \sin\theta_{\mathrm{d}} \\ z_5 \end{bmatrix} \tag{11}$$

where r_{door} denotes the rotation radius of the door; θ_{d} denotes the rotation angle of the door when reaching points $\boldsymbol{P}_5$, $\boldsymbol{P}_6$, and $\boldsymbol{P}_7$; and θ_{handle} denotes the rotation angle of the door when the mobile manipulator can pass through. It is noteworthy that points $\boldsymbol{P}_5$, $\boldsymbol{P}_6$, and $\boldsymbol{P}_7$ are calculated under the O_{door} coordinate system; in the trajectory planning of door opening, these points must be converted to the O_{body} coordinate system.

As shown in Fig. 1(d), Cur1 is a curve composed by Lin1, Arc1, and Arc2 in the Cartesian space under the O_{body} coordinate system. If we obtain $\boldsymbol{P}_1$, $\boldsymbol{P}_2$, $\boldsymbol{P}_3$, $\boldsymbol{P}_4$, $\boldsymbol{P}_5$, $\boldsymbol{P}_6$, and $\boldsymbol{P}_7$, then the trajectory of Cur1 can be planned by the proposed method.[30] The value r_{door}, the rotation radius of the door; the value r_{handle}, the rotation radius of the door handle; and the point $\boldsymbol{P}_2$ are known geometrical constraints or can be estimated.

The joint angles of manipulator are $q_{l1}, q_{l2}, q_{l3}, q_{l4}, q_{l5}, q_{l6}$, as shown in Fig. 2. The state vectors of the manipulator become

$$q_l = \begin{bmatrix} q_{l1} & q_{l2} & q_{l3} & q_{l4} & q_{l5} & q_{l6} \end{bmatrix}^T \tag{12}$$

The pose of the end effector is $\boldsymbol{P}_e$ $(x_{\mathrm{e}}, y_{\mathrm{e}}, z_{\mathrm{e}}, o_{\mathrm{e}}, a_{\mathrm{e}}, t_{\mathrm{e}})$. The state vectors of the pose become

$$P_e = [x_e \quad y_e \quad z_e \quad o_e \quad a_e \quad t_e]^T \tag{13}$$

The relationship between the pose of the robot's end effector and the joint angles of the manipulator is

$$P_e = J_{\mathrm{M}} q_l \tag{14}$$

where J_{M} is the manipulator Jacobian matrix.

3. Unknown-Force-Related Constraints Analysis and Estimate Scheme

As mentioned in Section 2, we use force/torque feedback-based control in the first and second steps, achieving compliance of the mobile base when the robot comes into contact with the handle. After

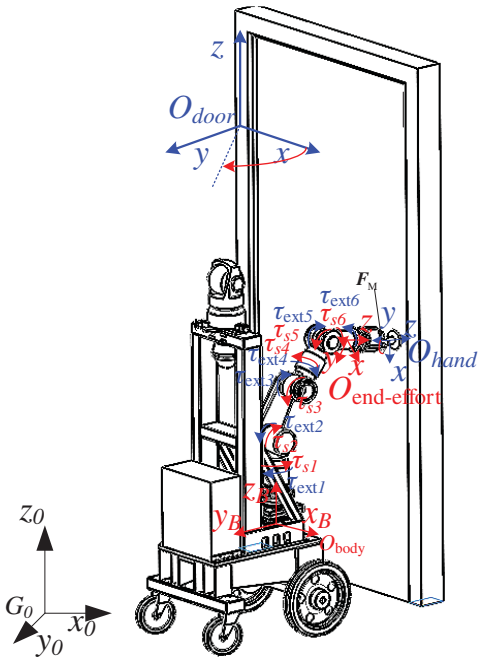

Fig. 3. Reference frames of the mobile manipulator during door opening.

the mobile manipulator, end effector has firmly grasped the handle, the mobile base will remain stable. In the third and fourth steps, called "turning the door handle" and "pulling the door", only the manipulator is used. As illustrated in the schematic diagram in Fig. 3, each module provides a rotary joint. Modules close to the mobile base are denoted as lower modules, and modules close to the end effector are called upper modules.

Referring to Liu, Goldenberg, and Zhang [18], we can consider the dynamics of the manipulator as follows:

For the first joint, $i = 1$,

$$\begin{aligned} &I_{l1}\ddot{q}_{l1} + f_{l1}(q_{l1}, \dot{q}_{l1}) + g_{l1}(q_{l1}) = \tau_{t1} + \tau_{ext1} \\ &I_{m1}\ddot{q}_{m1} + f_{m1}(q_{m1}, \dot{q}_{m1}) + \tfrac{\tau_{t1}}{N_1} = \tau_{m1} \end{aligned} \tag{15}$$

For the second joint, i =2,

$$\begin{aligned} &I_{l2}\ddot{q}_{l2} + f_{l2}(q_{l2}, \dot{q}_{l2}) + I_{l2}z_{l2}^T z_{l1}\ddot{q}_{l1} + g_{l2}(q_{l1}, q_{l2}) = \tau_{t2} + \tau_{ext2} \\ &I_{\mathrm{m}2}\ddot{q}_{m2} + f_{m2}(q_{m2}, \dot{q}_{m2}) + I_{m2}z_{m2}^T z_{l1}\ddot{q}_{l1} + \tfrac{\tau_{t2}}{N_2} = \tau_{m2} \end{aligned} \tag{16}$$

For the upper joints, $i \geq 3$,

$$\begin{aligned} &I_{li}\ddot{q}_{li} + f_{li}(q_{li}, \dot{q}_{li}) + I_{li}\sum_{j=1}^{i-1} z_{li}^T z_{lj}\ddot{q}_{lj} + I_{li}\sum_{j=2}^{i-1}\sum_{k=1}^{j-1} z_{li}^T(z_{lk} \times z_{lj})\dot{q}_{lk}\dot{q}_{lj} + g_{li}(q_{l1}, \cdots, q_{li}) = \tau_{ti} + \tau_{exti} \\ &I_{mi}\ddot{q}_{mi} + f_{mi}(q_{mi}, \dot{q}_{mi}) + I_{mi}\sum_{j=1}^{i-1} z_{mi}^T z_{lj}\ddot{q}_{lj} + I_{mi}\sum_{j=2}^{i-1}\sum_{k=1}^{j-1} z_{mi}^T(z_{mk} \times z_{mj})\dot{q}_{mk}\dot{q}_{mj} + \tfrac{\tau_{ti}}{N_i} = \tau_{mi} \end{aligned} \tag{17}$$

The geometric parameters of the manipulator are summarized in Table III.

The link-side friction $f_{li}(q_{li}, \dot{q}_{li})$ is assumed to be a function of the link position and velocity as in ref. [17]:

$$f_{li}(q_{li}, \dot{q}_{li}) = (f_{lci} + f_{lsi}\exp(-f_{l\tau i}\dot{q}_{li}^2))\mathrm{sgn}(\dot{q}_{li}) + b_{li}\dot{q}_{li} + f_{qli}(q_{li}, \dot{q}_{li}) \tag{18}$$

Table III. Geometric and inertial parameters for the manipulator.

Symbol	Description
I_{mi}	Moment of inertia of the ith rotor about the axis of rotation
I_{li}	Moment of inertia of the ith link about the axis of rotation
N_i	Reduction ratio of the speed reducer
q_{mi}	Motor position of the ith joint
q_{li}	Link position of the ith joint
$f_{mi}(q_{mi}, \dot{q}_{mi})$	Joint friction on motor side, assumed to be a function of motor position and velocity
$f_{li}(q_{li}, \dot{q}_{li})$	Joint friction on link side, assumed to be a function of link position and velocity
$g_{li}(q_{l0} \cdots q_{li})$	Link gravity of the ith joint
τ_{exti}	External torque added to the link of the ith joint
τ_{ti}	Torque transferred at the transmission system of the ith joint
τ_{mi}	Motor output torque of the ith joint
z_{mi}	Unity vector along the axis of rotation of the ith joint
z_{li}	Unity vector along the axis of rotation of the ith link

Similarly, the rotor-side friction can be modeled as

$$f_{mi}(q_{mi}, \dot{q}_{mi}) = (f_{mci} + f_{msi} \exp(-f_{m\tau i}\dot{q}_{mi}^2))\mathrm{sgn}(\dot{q}_{mi}) + b_{mi}\dot{q}_{mi} + f_{qmi}(q_{mi}, \dot{q}_{mi}) \tag{19}$$

where f_{lci} and f_{mci} denote the Coulomb friction-related parameters on the link side and motor side; similarly, f_{lsi} and f_{msi} represent the static-friction-related parameters; $f_{l\tau i}$ and $f_{m\tau i}$ are positive parameters corresponding to the Stribeck effect; b_{li} and b_{mi} denote the viscous friction coefficients; and $f_{qli}(q_{li}, \dot{q}_{li})$ and $f_{qmi}(q_{mi}, \dot{q}_{mi})$ reflect the position dependency of friction and other friction-modeling errors.

The torque constraint from the external torque τ_{ext} can be expressed in terms of a generalized multiplier $F_{\mathrm{M}} \in R^{6\times 1}$ according to

$$\tau_{ext} = J_{\mathrm{M}}^T F_{\mathrm{M}} \tag{20}$$

where F_{M} denotes external force/torque from the operation object and J_{M}^T is the manipulator Jacobian matrix.

The torque constraint from the coupling torque τ_s is caused by the relative motion of links, such as gravity, the centrifugal force, and the Coriolis force. Define the internal force at the joint as $\tau_{\mathrm{iner}} = \tau_{\mathrm{ext}} - \tau_{\mathrm{s}}$ as shown in Fig. 3. τ_{iner} denotes the internal torque. Therefore, the dynamics of the manipulator can be rewritten as follows:

For the first joint, $i = 1$,

$$I_1(\ddot{q}_{l1}, \ddot{q}_{m1}) + f_{m1}(q_{m1}, \dot{q}_{m1}) - \frac{\tau_{\mathrm{iner1}}}{N_1} = \tau_{m1} \tag{21}$$

where $I_1(\ddot{q}_{l1}, \ddot{q}_{m1}) = \frac{I_{l1}\ddot{q}_{l1} + N_1 I_{m1}\ddot{q}_{m1}}{N_1}$.

For the second joint, $i = 2$,

$$I_2(\ddot{q}_{l2}, \ddot{q}_{m2}) + f_{m2}(q_{m2}, \dot{q}_{m2}) + z_{m2}(\ddot{q}_{l1}) - \frac{\tau_{\mathrm{iner2}}}{N_2} = \tau_{m2} \tag{22}$$

where $I_2(\ddot{q}_{l2}, \ddot{q}_{m2}) = \frac{I_{l2}\ddot{q}_{l2} + N_2 I_{\mathrm{m}2}\ddot{q}_{m2}}{N_2}$, $z_{m2}(\ddot{q}_{l1}) = I_{m2} z_{m2}^T z_{l1}\ddot{q}_{l1}$.

For the upper joints, $i \geq 3$

$$I_i(\ddot{q}_{li}, \ddot{q}_{mi}) + f_{mi}(q_{mi}, \dot{q}_{mi}) + z_{mi}(\ddot{q}_{li}) + z_{mkj}(\dot{q}_{mk}, \dot{q}_{mj}) - \frac{\tau_{\mathrm{iner}i}}{N_i} = \tau_{mi} \tag{23}$$

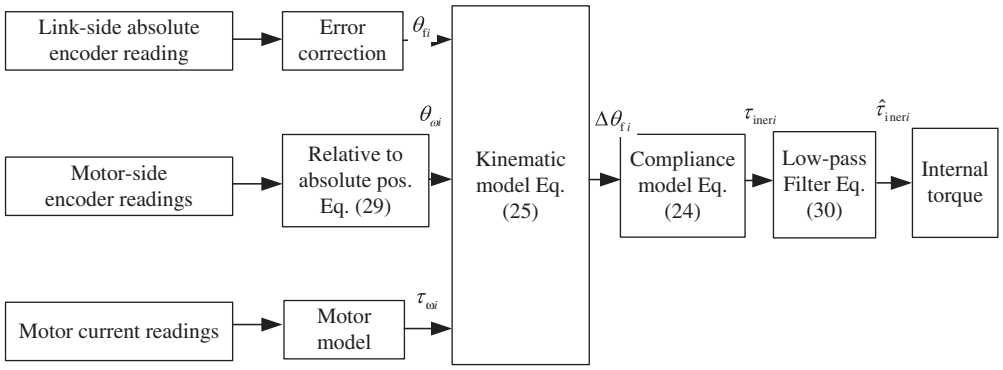

Fig. 4. Block diagram of the torque estimation technique.

where $I_i(\ddot{q}_{li}, \ddot{q}_{mi}) = \frac{I_{li}\ddot{q}_{li} + N_i I_{mi}\ddot{q}_{mi}}{N_i}$, $z_{mi}(\ddot{q}_{li}) = I_{mi}\sum_{j=1}^{i-1} z_{mi}^T z_{lj}\ddot{q}_{lj}$, $z_{mkj}(\dot{q}_{mk}, \dot{q}_{mj}) = I_{mi}\sum_{j=2}^{i-1}$ $\sum_{k=1}^{j-1} z_{mi}^T(z_{mk} \times z_{mj})\dot{q}_{mk}\dot{q}_{mj}$.

Traditionally, torque sensors can be used to measure the internal force τ_{iner}, but the extreme physical constraints may cause conventional force/torque sensors without protection to stop working. Furthermore, when force/torque sensors are protected, their weight is greatly increased and precision is reduced. It is difficult and expensive for heavy force/torque sensors to be assembled in a multi-joint manipulator. Furthermore, the estimation error may then be large, leading to large internal forces. Thus, we estimate the internal force at a joint τ_{iner} as in refs. [8, 30].

The internal torque τ_{iner} at a joint can be estimated using the motor current and the link-side and motor-side encoders. From the literature,[29] $\boldsymbol{\tau}_{iner\text{i}}$ can be defined as

$$\tau_{\text{iner}i} = \frac{\tan(\Delta\theta_{\text{f}i} c_{\text{f}i} K_{\text{f}i})}{c_{\text{f}i}} \tag{24}$$

where $c_{\text{f}i}$ and $K_{\text{f}i}$ are constant parameters, and $\Delta\theta_{\text{f}i}$ can be modified as

$$\Delta\theta_{\text{f}i} = \Delta\theta_i + \frac{\text{sgn}(\tau_{\omega i})}{c_{\omega i} N_i K_{\omega i}}(1 - e^{-c_{\omega i}|\tau_{\omega i}|}) - \theta_{\text{err}i} \tag{25}$$

where $c_{\omega i}$ and $K_{\omega i}$ are constant parameters and $\tau_{\omega i}$ is approximated by the ith motor model of the current.

The joint-deformation angle $\Delta\theta_i$ can be defined as

$$\Delta\theta_i = \theta_{\text{f}i} - \theta_{\omega i} \tag{26}$$

where $\theta_{\text{f}i}, \theta_{\omega i}$ denote the link-side and motor-side angles, respectively.

Kinematic error $\theta_{\text{err}i}$ can be written as

$$\begin{aligned}\theta_{\text{err}i} = {} & a_{0i} + a_{l1i}\cos(\theta_{fi}\omega_{li}) + b_{l1i}\sin(\theta_{fi}\omega_{li}) + a_{\omega 1i}\cos(\theta_{\omega i}\omega_{\omega i}) + b_{\omega 1i}\sin(\theta_{\omega i}\omega_{\omega i}) \\ & + a_{\omega 2i}\cos(2\theta_{\omega i}\omega_{\omega i}) + b_{\omega 2i}\sin(2\theta_{\omega i}\omega_{\omega i})\end{aligned} \tag{27}$$

where $a_{0i}, a_{l1i}, b_{l1i}, \omega_{li}, a_{\omega 1i}, b_{\omega 1i}, a_{\omega 2i}, b_{\omega 2i}, \omega_{\omega i}$ are constant parameters.

A block diagram illustrating the joint estimation method for internal force τ_{iner} is shown in Fig. 4.

Joints are usually equipped with optical incremental encoders to measure motor-side position for control purposes. However, incremental encoders provide only the relative position of the motor shaft. Therefore, a method for determining the absolute position of the motor shaft is necessary. To obtain the motor's absolute position, the joint is rotated 360° clockwise (free-running) while the flexspline output position is recorded at each encountered index of the incremental encoder $\theta_{fo}^{c\omega_{\text{i}}}$. Then the joint is rotated 360° counterclockwise, and the link-side absolute encoder readings at each index $\theta_{fo}^{cc\omega_{\text{i}}}$ are recorded. For one complete rotation, there are N indices. The offset of the incremental encoder

installed motor-side is determined as

$$\theta_{\text{offset}} = \sum_{i=0}^{N-1} \frac{\theta_{fo}^{c\omega_i} + \theta_{fo}^{cc\omega_i} - 2i360/N}{2N} \tag{28}$$

where θ_{offset} is the offset between the link-side absolute position measurement and the motor-side incremental encoder relative position measurement, N is the gear ratio, which equals the number of indices.

The absolute position of the motor shaft is estimated using the recorded link-side positions θ_{fo0}, at the first encountered index after power-on as

$$\theta_{\omega \text{i}} = \theta_{\text{offset}} + \frac{360}{N} \text{int}\left(\frac{N}{360}(\theta_{fo0} - \theta_{\text{offset}}) + 0.5\right) + \theta_{IE} \tag{29}$$

where θ_{IE} is the incremental encoder reading and int$(\cdot)$ is a conversion function that converts floating-point numbers to the integer data type.

A detailed description of how to determine the coefficients of the harmonic drive compliance model is presented in ref. [8] The discrete-time implementation and the parameters of the low-pass filter shown in Fig. 4 are given by

$$\hat{\tau}_{\text{ineri}}[i] = 0.95\hat{\tau}_{\text{ineri}}[i-1] + 0.025\tau_{\text{ineri}}[i] + 0.025\tau_{\text{ineri}}[i-1] \tag{30}$$

where $\hat{\tau}_{\text{ineri}}$ is the filtered torque estimate, and τ_{ineri} is the estimated torque from the model and the readings of both encoders.

4. Design of a Robust Adaptive Control Strategy

During this process, a robust adaptive control algorithm is used to track the planning trajectory Cur1 to open the door. For the manipulator, each joint is considered as an independent subsystem, and the mainly dynamic effects from the other links and joints are treated as coupling torque τ_s. The joint estimation errors are treated as disturbances.

In Eqs. (21)–(23), the internal force τ_{ineri} at the joint can be measured by the proposed method online. Joint friction is another major source of model uncertainty. The friction model parameters b_i, f_{ci}, f_{si}, and $f_{\tau i}$ are not accurately known, and not necessarily constant. However, their nominal values can be determined offline as constants. The nominal values of b_i, f_{ci}, f_{si}, and $f_{\tau i}$ are denoted as $\hat{b}_i$, $\hat{f}_{ci}$, $\hat{f}_{si}$, and $\hat{f}_{\tau i}$, respectively.

Let $F_i = [\, b_i \quad f_{ci} \quad f_{si} \quad f_{\tau i} \,]^T$. According to the model uncertainty decomposition scheme proposed in ref. [17], F_i can be decomposed into a constant part plus a variable part

$$F_i = F_i^c + F_i^v \tag{31}$$

where the superscripts "c" and "v" represent constant and variable parts, respectively.

Property 1: The variable part in Eq. (31) is bounded, i.e.,

$$\left|F_i^v\right| < \rho_{F_i} \tag{32}$$

where ρ_{F_i} is the constant bound.

Property 2: The non-parametric friction term in Eq. (19) is bounded, i.e.,

$$\left|f_{qmi}(q_{mi}, \dot{q}_{mi})\right| < \rho_{f_{mi}} \tag{33}$$

where $\rho_{f_{mi}}$ is a known constant bound for any positions and velocities of joints.

Property 3: Because z_i, z_j, and z_k are unit vectors, the resulting vector products $z_i^T(z_k \times z_j)$ and $z_i^T z_j$ are bounded. Furthermore, as the mobile base is stabilized, the accelerations $\ddot{q}_{lj}$ and velocities

$(\dot{q}_{mj}, \dot{q}_{mk})$ must be bounded. Hence, the inertial and Coriolis forces associated with motion of the base robotic arm are bounded; i.e., if we define

$$\rho_{\alpha_{\text{base}}} > \max \left| z_{mi}(\ddot{q}_{li}) + z_{mkj}(\dot{q}_{mk}, \dot{q}_{mj}) \right| \tag{34}$$

for any possible configuration, then

$$|\tau_{\text{base}i}| = I_i \left| z_{mi}(\ddot{q}_{li}) + z_{mkj}(\dot{q}_{mk}, \dot{q}_{mj}) \right| < I_i \rho_{\text{base}} \tag{35}$$

where ρ_{base} is a constant bound.

Property 4: The torque estimation inaccuracy and noise is bounded; furthermore, the estimated error of $\tau_{\text{iner}i}$ is bounded, i.e.,

$$|\tilde{\tau}_{\text{iner}i}| = |\tau_{\text{iner}i} - \hat{\tau}_{\text{iner}i}| < \rho_{\tau_{\text{iner}i}} \tag{36}$$

where $\tilde{\tau}_{\text{iner}i}$ is the torque estimation and $\rho_{\tau_{\text{iner}i}}$ are known constant bounds.

Define the system errors as

$$e_i = q_{li} - q_{li}^d \tag{37}$$

$$r_i = \dot{e}_i + \lambda_i e_i \tag{38}$$

$$a_i = \ddot{q}_{li}^d - 2\lambda_i \dot{e}_i - \lambda_i^2 e_i \tag{39}$$

where q_{li}^d is the desired joint space motion for the ith joint; $\dot{q}_{li}^d$ denotes the corresponding joint-space velocity; $\ddot{q}_{li}^d$ represents the desired joint-space acceleration; and q_{li}^d, $\dot{q}_{li}^d$, $\ddot{q}_{li}^d$ are known from the proposed planning trajectory. λ_i is a positive constant. Let $\hat{b}_i^c$, $\hat{f}_{ci}^c$, $\hat{f}_{si}^c$, and $\hat{f}_{\tau i}^c$ represent estimates of the constant friction parameters; using the linearization scheme proposed in ref. [5], the friction model shown in Eqs. (21)–(23) can be approximated by

$$|f_{mi}(q_{mi}, \dot{q}_{mi})| \cong f_{mi}^c(\dot{q}_{mi}) + \hat{Y}_i(\dot{q}_{mi})(\tilde{F}_i^c + \tilde{F}_i^v) + f_{mqi}(q_{mi}, \dot{q}_{mi}) + \tilde{f}_{mi}(\dot{q}_{mi}) \tag{40}$$

where $\tilde{F}_i^c = F_i^c - \hat{F}_i^v$ with $\hat{F}_i^c = [\,\hat{b}_i^c \quad \hat{f}_{ci}^c \quad \hat{f}_{si}^c \quad \hat{f}_{\tau i}^c\,]^T$; $f_{mi}^c(\dot{q}_{mi})$, $\tilde{f}_{mi}(\dot{q}_{mi})$, and $Y_i(\dot{q}_{mi})$ can be defined as follows:

$$\hat{f}_{mi}^c(\dot{q}_{mi}) = \left[\hat{f}_{ci}^c + \hat{f}_{si}^c \exp(-\hat{f}_{\tau i}^c \dot{q}_{mi}^2)\right] \text{sat}(\dot{q}_{mi}, \varepsilon_{\dot{q}_{mi}}) + \hat{b}_i^c \dot{q}_{mi} \tag{41}$$

$$\tilde{f}_{mi}(\dot{q}_{mi}) = \left[f_{ci} + f_{si} \exp(-f_{\tau i} \dot{q}_{mi}^2)\right] \left[\text{sgn}(\dot{q}_{mi}) - sat(\dot{q}_{mi}, \varepsilon_{\dot{q}_{mi}})\right] \tag{42}$$

$$\hat{Y}_{mi}(\dot{q}_{mi}) = \left[0 \quad 1 \quad \exp(-\hat{f}_{\tau i}^c \dot{q}_{mi}^2) \quad -\hat{f}_{si}^c \dot{q}_{mi}^2 \exp(-\hat{f}_{\tau i}^c \dot{q}_{mi}^2)\right] \cdot \text{sat}(\dot{q}_{mi}, \varepsilon_{\dot{q}_{mi}}) + \left[\dot{q}_{mi} \quad 0 \quad 0 \quad 0\right] \tag{43}$$

where $\varepsilon_{\dot{q}_{mi}}$ are positive constants, and $\text{sat}(\dot{q}_{mi}, \varepsilon_{\dot{q}_{mi}})$ is the saturation function defined as follows:

$$\text{sat}(\dot{q}_{mi}, \varepsilon_{\dot{q}_{mi}}) = \begin{cases} \frac{\dot{q}_{mi}}{|\dot{q}_{mi}|} & |\dot{q}_{mi}| > \varepsilon_{\dot{q}_{mi}} \\ \frac{\dot{q}_{mi}}{\varepsilon_{\dot{q}_{mi}}} & |\dot{q}_{mi}| \le \varepsilon_{\dot{q}_{mi}} \end{cases} \tag{44}$$

Property 5: The last item in Eq. (40), $\tilde{f}_{mi}(\dot{q}_{mi})$, is bounded, i.e., $|\tilde{f}_{mi}(\dot{q}_{mi})| < \rho_{f_i}$.

A robust adaptive control law is designed as

$$\begin{aligned} \tau_{mi} = {} & I_i a_i + \tfrac{\hat{\tau}_{\text{iner}i}}{N_i} + \hat{f}_{mi}^c(\dot{q}_{mi}) - K_{Ii} \textstyle\int_0^t r_i(t)\mathrm{d}t - \left(\rho_{\text{F}_i} + \rho_{f_{mi}} + I_i \rho_{base} + \tfrac{\rho_{\tau_{\text{iner}i}}}{N_i}\right) \cdot \text{sat}(r_i, \varepsilon_{ri}) \\ & - \sum_{j=1}^{4} \{\rho_{\text{F}_{ij}} \hat{Y}_{ij}(\dot{q}_{mi}) \text{sat}(r_i \hat{Y}_{ij}(\dot{q}_{mi}), \varepsilon_{F_{ij}})\} \end{aligned} \tag{45}$$

where $\hat{Y}_{ij}(\dot{q}_{mi})$ is the jth element of $\hat{Y}_i(\dot{q}_{mi})$ and ε_{ri} and $\varepsilon_{F_{ij}}$ are positive control parameters.

Theorem 1: For the joint dynamics as given in Eqs. (21)–(23), the tracking error of each joint is uniformly bounded under the control law given by Eq. (45) and the adaption law of $\dot{\hat{F}}_i^c = -\mu_{F_{ic}}[\hat{Y}_i(\dot{q}_{mi})]^T r_i$ with a positive constant $\mu_{F_{ic}}$.

Proof 1: Consider the Lyapunov function candidate

$$V = \frac{1}{2} I_i r_i^2 + \frac{1}{2} k_{Ii} \left[\int_0^t r_i(t) \mathrm{d}t \right]^2 + \frac{1}{2} \frac{(\tilde{F}_i^c)^T \tilde{F}_i^c}{\mu_{F_{ic}}} \tag{46}$$

Differentiating Eq. (46) yields

$$\dot{V} = r_i \{ I_i \dot{r}_i + k_{Ii} \int_0^t r_i(t) \mathrm{d}t \} + \frac{(\dot{\tilde{F}}_i^c)^T \tilde{F}_i^c}{\mu_{F_{ic}}} \tag{47}$$

Substituting Eqs. (40) and (45) into Eq. (47), we obtain

$$\begin{aligned} r_i \{ I_i \dot{r}_i + k_{Ii} \textstyle\int_0^t r_i(t) \mathrm{d}t \} = & -\mathrm{I}_i \lambda_i r_i^2 - r_i f_{mi}(q_{mi}, \dot{q}_{mi}) - r_i \tau_{\mathrm{base}i} \\ & - r_i \left[\frac{\tilde{\tau}_{\mathrm{iner}i} + \rho_{\tau_{\mathrm{iner}i}} \mathrm{sat}(r_i, \varepsilon_{ri})}{N_i} \right] - r_i (\rho_{f_i} + \rho_{f_{mi}} + \mathrm{I}_i \rho_{\mathrm{base}}) \mathrm{sat}(r_i, \varepsilon_{ri}) \\ & - r_i \sum_{j=1}^{4} \{ \rho_{F_{ij}} \hat{Y}_{ij}(\dot{q}_{li}) \cdot \mathrm{sat}(r_i \hat{Y}_{ij}(\dot{q}_{li}), \varepsilon_{F_{ij}}) \} + r_i \hat{f}_{mi}^c(\dot{q}_{mi}) \end{aligned} \tag{48}$$

Because F_i^c is a constant vector, we have

$$\dot{\tilde{F}}_i^c = -\dot{\hat{F}}_i^c \tag{49}$$

Substituting Eq. (39) and the adaption law into Eq. (48), and considering the saturation function Eq. (44), we can obtain

$$\begin{aligned} \dot{V} = & -\mathrm{I}_i \lambda_i r_i^2 - r_i \left[\tilde{f}_{mi}(\dot{q}_{mi}) + \rho_{f_i} \mathrm{sat}(r_i, \varepsilon_{ri}) \right] - \frac{r_i \left[\tilde{\tau}_{\mathrm{iner}i} + \rho_{\tau_{\mathrm{iner}i}} \mathrm{sat}(r_i, \varepsilon_{ri}) \right]}{N_i} \\ & - r_i \left[f_{mqi}(q_{mi}, \dot{q}_{mi}) + \rho_{f_{mi}} \mathrm{sat}(r_i, \varepsilon_{ri}) \right] - r_i \left[\tau_{\mathrm{base}i} + \mathrm{I}_i \rho_{\mathrm{base}} \mathrm{sat}(r_i, \varepsilon_{ri}) \right] \\ & - \sum_{j=1}^{4} r_i \hat{Y}_{ij}(\dot{q}_{mi}) \left[F_{ij}^v + \rho_{F_{ij}} \mathrm{sat}(r_i \hat{Y}_{ij}(\dot{q}_{mi}), \varepsilon_{F_{ij}}) \right] \Bigg\} \end{aligned} \tag{50}$$

where F_{ij}^v and $\rho_{F_{ij}}$ are the jth elements of F_i^v and ρ_{F_i}, respectively.

From **Property 1–5**, if $|r_i| > \varepsilon_{ri}$, then the second to fifth items in Eq. (50) are negative, i.e.,

$$-r_i \left[\tilde{f}_{mi}(\dot{q}_{mi}) + \rho_{f_i} \cdot \mathrm{sat}(r_i, \varepsilon_{ri}) \right] < 0 \tag{51}$$

$$-r_i \left[\tilde{\tau}_{\mathrm{iner}i} + \rho_{\tau_{\mathrm{iner}i}} \cdot \mathrm{sat}(r_i, \varepsilon_{ri}) \right] < 0 \tag{52}$$

$$-r_i \left[f_{mqi}(q_{mi}, \dot{q}_{mi}) + \rho_{f_{mi}} \cdot \mathrm{sat}(r_i, \varepsilon_{ri}) \right] < 0 \tag{53}$$

$$-r_i \left[\tau_{\mathrm{base}i} + I_i \rho_{\alpha_{\mathrm{base}}} \cdot \mathrm{sat}(r_i, \varepsilon_{ri}) \right] < 0 \tag{54}$$

If $|r_i| \leq \varepsilon_{ri}$, we have

$$-r_i\left[\tilde{f}_{mi}(\dot{q}_{mi}) + \rho_{f_i} \cdot \mathrm{sat}(r_i, \varepsilon_{ri})\right] \leq \rho_{f_i} r_i \left\{\frac{r_i}{|r_i|} - \frac{r_i}{\varepsilon_{ri}}\right\} \tag{55}$$

$$-r_i\left[\tilde{\tau}_{\mathrm{iner}i} + \rho_{\tau_{\mathrm{iner}i}} \cdot \mathrm{sat}(r_i, \varepsilon_{ri})\right] < \rho_{\tau_{\mathrm{iner}i}} r_i \left\{\frac{r_i}{|r_i|} - \frac{r_i}{\varepsilon_{ri}}\right\} \tag{56}$$

$$-r_i\left[f_{mqi}(q_{mi}, \dot{q}_{mi}) + \rho_{f_{mi}} \cdot \mathrm{sat}(r_i, \varepsilon_{ri})\right] \leq \rho_{f_{mi}} r_i \left\{\frac{r_i}{|r_i|} - \frac{r_i}{\varepsilon_{ri}}\right\} \tag{57}$$

$$-r_i\left[\tau_{\mathrm{base}i} + I_i \rho_{\alpha_{\mathrm{base}}} \cdot \mathrm{sat}(r_i, \varepsilon_{ri})\right] \leq I_i \rho_{\alpha_{\mathrm{base}}} r_i \left\{\frac{r_i}{|r_i|} - \frac{r_i}{\varepsilon_{ri}}\right\} \tag{58}$$

Similarly, from **Property 1–5**, if $|r_i \hat{Y}_{ij}(\dot{q}_{mi})| > \varepsilon_{F_{ij}}$, then the last item in Eq. (50) satisfies

$$-r_i \hat{Y}_{ij}(\dot{q}_{mi})\left[F_{ij}^{v} + \rho_{F_{ij}} \mathrm{sat}(r_i \hat{Y}_{ij}(\dot{q}_{mi}), \varepsilon_{F_{ij}})\right] < 0 \tag{59}$$

If $|r_i \hat{Y}_{ij}(\dot{q}_{mi})| \leq \varepsilon_{F_{ij}}$, we have

$$-r_i \hat{Y}_{ij}(\dot{q}_{mi})\left[F_{ij}^{v} + \rho_{F_{ij}} \mathrm{sat}(r_i \hat{Y}_{ij}(\dot{q}_{mi}), \varepsilon_{F_{ij}})\right] < \rho_{F_{ij}} r_i \hat{Y}_{ij}(\dot{q}_{mi}) \left\{\frac{r_i \hat{Y}_{ij}(\dot{q}_{mi})}{|r_i \hat{Y}_{ij}(\dot{q}_{li})|} - \frac{r_i \hat{Y}_{ij}(\dot{q}_{mi})}{\varepsilon_{F_{ij}}}\right\} \tag{60}$$

Because the maximum values are $|r_i| = \frac{\varepsilon_{ri}}{2}$ and $|r_i \hat{Y}_{ij}(\dot{q}_{mi})| = \frac{\varepsilon_{F_{ij}}}{2}$, respectively, we can obtain

$$\dot{V} \leq -I_i \lambda_i r_i^2 + \sum_{j=1}^{4} \frac{\rho_{F_{ij}} \varepsilon_{F_{ij}}}{4} + \frac{\varepsilon_{ri}}{4}\left(\rho_{f_i} + \frac{\rho_{\tau_{\mathrm{iner}i}}}{N_i} + \rho_{f_{mi}} + I_i \rho_{\alpha_{\mathrm{base}}}\right) \tag{61}$$

From Eq. (51), V is a Lyapunov function only when

$$|r_i| > \sqrt{\frac{\frac{\varepsilon_{ri}}{4}\left(\rho_{f_i} + \frac{\rho_{\tau_{\mathrm{iner}i}}}{N_i} + \rho_{f_{mi}} + I_i \rho_{\alpha_{\mathrm{base}}}\right) + \sum_{j=1}^{4} \frac{\rho_{F_{ij}} \varepsilon_{F_{ij}}}{4}}{I_i \lambda_i}} \tag{62}$$

Define $S = \{r_i \in \Re | r_i^2 \leq \frac{\varepsilon_{ri}(\rho_{f_i} + \frac{\rho_{\tau_{\mathrm{iner}i}}}{N_i} + \rho_{f_{mi}} + \mathrm{I}_i \rho_{\alpha_{\mathrm{base}}}) + \sum_{j=1}^{4} \frac{\rho_{F_{ij}} \varepsilon_{F_{ij}}}{2}}{I_i \lambda_i}\}$; on the surface of S, ∂S, we have

$$\dot{V} \leq -\left\{\sum_{j=1}^{4} \frac{\rho_{F_{ij}} \varepsilon_{F_{ij}}}{4} + \frac{\varepsilon_{ri}}{4}\left(\rho_{f_i} + \frac{\rho_{\tau_{\mathrm{iner}i}}}{N_i} + \rho_{f_{mi}} + \mathrm{I}_i \rho_{\alpha_{\mathrm{base}}}\right)\right\} \tag{63}$$

Denote t_s as the time for the solution trajectory to intersect the surface ∂S, then

$$t_s \leq \frac{V(r_i(0)) - V(r_i(t_s))}{\frac{\varepsilon_{ri}}{4}\left(\rho_{f_i} + \frac{\rho_{\tau_{\mathrm{iner}i}}}{N_i} + \rho_{f_{mi}} + \mathrm{I}_i \rho_{\alpha_{\mathrm{base}}}\right) + \sum_{j=1}^{4} \frac{\rho_{F_{ij}} \varepsilon_{F_{ij}}}{4}} \tag{64}$$

Therefore, r_i is bounded, which indicates that e_i and $\dot{e}_i$ are bounded as per the proof.

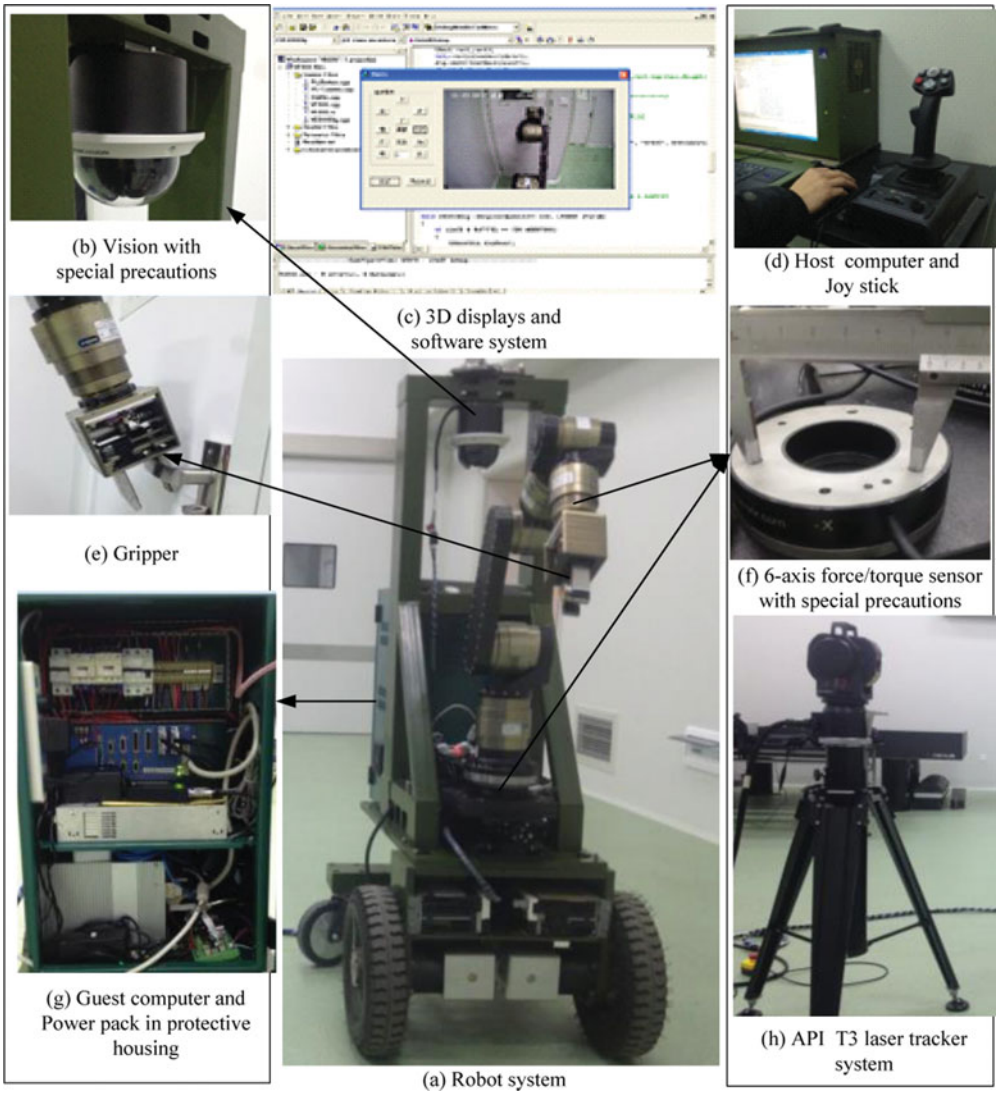

Fig. 5. Software and hardware for the mobile manipulator HITRMM-1.

5. Experimental Results

5.1. The experimental platform

The robotic platform, called HITRMM-1, was assembled in early 2014 by the authors (see Fig. 5). It consisted of a six-DOF arm LWA4/SDH and a four-wheeled mobile base with two active wheels (front) and two passive wheels (back). For this work, a gripper with two fingers was used as the end effector. The mobile manipulator was equipped with several distinct types of sensors. The mobile manipulator measured forces and torques using a wrist-mounted six-axis force/torque sensor to monitor the forces applied to the wrist, and a base-mounted six-axis force/torque sensor to achieve mobile base compliance control. The six-axis force/torque sensors all had special protection. A joystick with associated force feedback control from the base-mounted six-axis force/torque sensor was used for tele-operation to avoid harm to human health from extreme physical conditions. The API T3 (AUTOMATED PRECISION INC.) laser tracker system was used to aid in the experiment to measure the real rotation radius of the handle r_{handle} and the door r_{door}. The mobile manipulator's joints also sensed motor-side position, link-side position, motor-side velocity, and motor-side current, which were used for control. HITRMM-1 was designed for working in simulated rescue environments with extreme physical conditions (60°C, relative humidity of 300%, and equivalent radiation of 1 mSv/h).

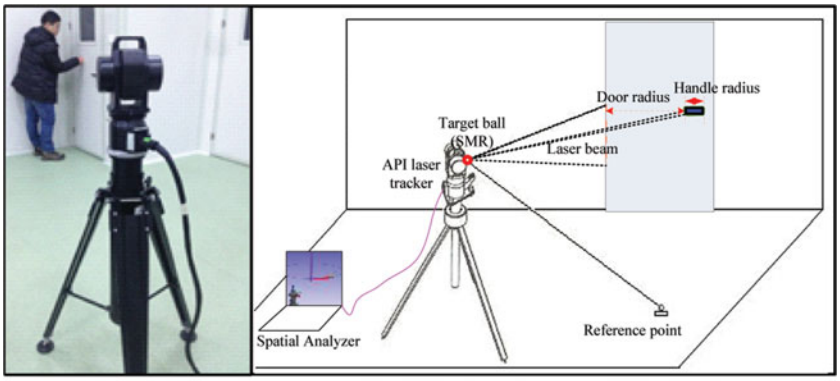

Fig. 6. (a) Reference tested by API tracking system; (b) schematic diagram.

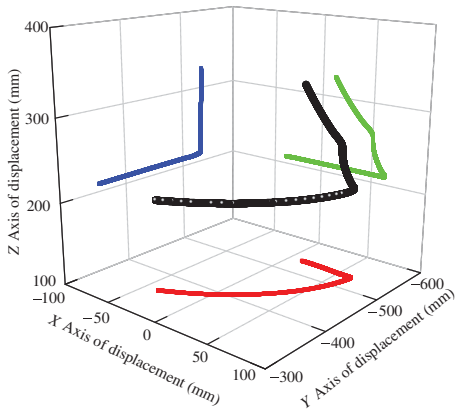

Fig. 7. Planning position of end effector in O_{body}.

5.2. Door-opening experiment

At this stage, a real-life door with spring-loaded handle hinge and door hinge was used for the door-opening experiment. Experiments were carried out in a simulated rescue environment approximating a nuclear power plant accident (55°C, relative humidity of 300%, equivalent radiation of 1 mSv/h). The API III laser tracker system tested the real rotation radius of handle r_{handle} and door r_{door} as shown in Fig. 6(a). The schematic diagram of the test process is shown in Fig. 6(b). The desired trajectory during door opening was calculated online by the onboard computer. Using the Hermite Cubic Polynomial method, we can plan the continuous position trajectory. In addition, we can obtain the continuous orientation trajectory generated by interpolating key orientations with the spherical spline quaternion interpolation method. This process is realized by C++ programming with a cycle of 20 ms. The planning trajectory for opening the door in the O_{body} coordinate system is shown in Figs. 7 and 8 ref. [27].

By inverse kinematics, we can obtain the joint position sequence, and using the joint trajectory smoothing generation method, we can obtain the continuous trajectory of position, angular velocity, and angular acceleration of the joints. This process is realized by C++ programming with a cycle of 20 ms. The reading of position, angular velocity, and angular acceleration of the joints in the joint space are shown in Figs. 9–11.

To this end, several results were confirmed. Two types of experiments were performed. For Type (a), we used the method proposed in ref. [32] according to the planning trajectory of the joints to realize position control. For Type (b), we used the proposed method in this study. The design parameters and control parameters are detailed in Tables IV and V. The desired trajectories of the HITRMM-1 joints during door opening were calculated online by the onboard computer with a cycle

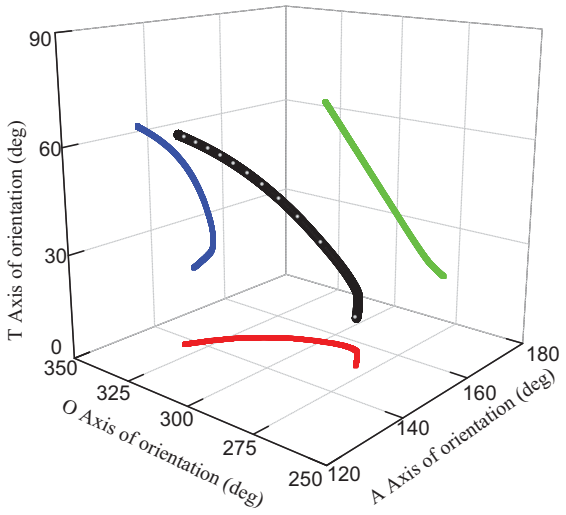

Fig. 8. Planning orientation of end effector in O_{body}.

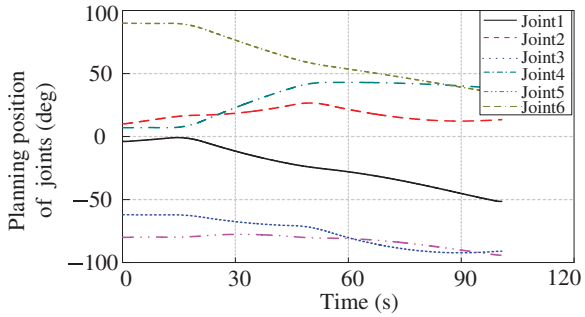

Fig. 9. Planning position of joints.

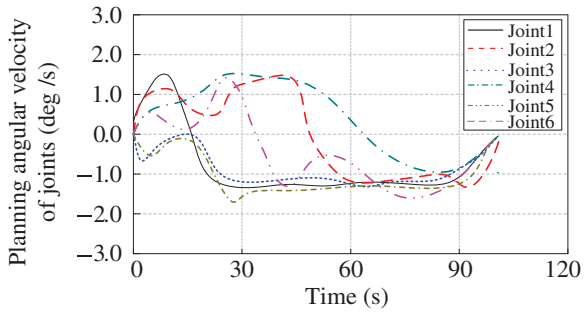

Fig. 10. Planning angular velocity of joints.

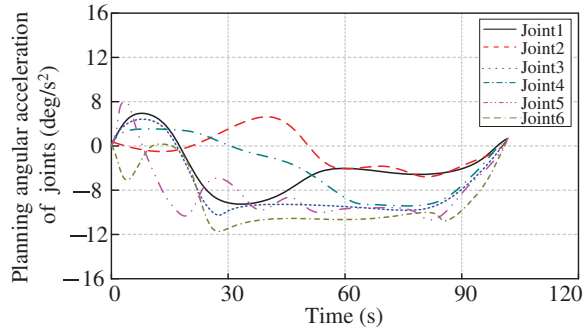

Fig. 11. Planning angular acceleration of joints.

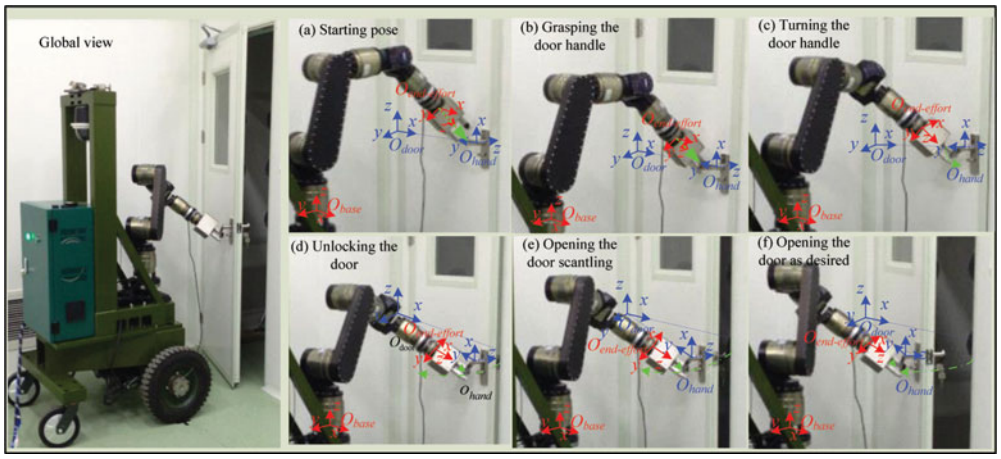

Fig. 12. Sequence of the door-opening experiment.

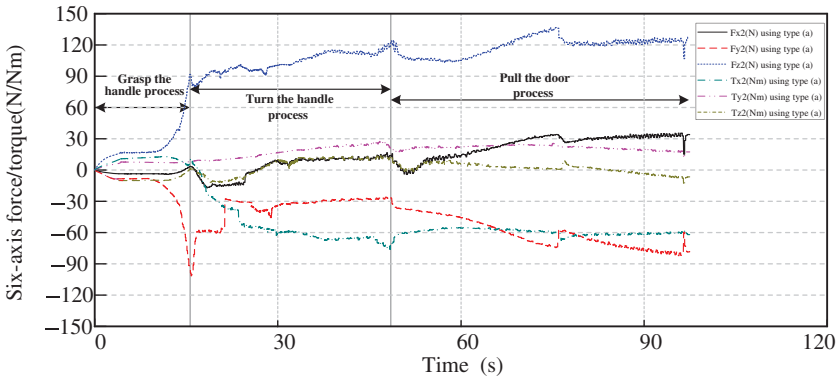

Fig. 13. Six-axis force/torque measurements of the wrist with Type (a).

of 20 ms, as shown in Figs. 9-11. The force-related constraints were estimated by the proposed position measurements method. This control loop is realized by C++ programming with a cycle of 50 ms. The process of the experiment for door opening is shown in Fig. 12.

Figure 13 shows the six-axis force/torque measurements of the wrist using Type (a). Figure 14 shows the six-axis force/torque measurements of the wrist using Type (b). The six-axis force/torque measurements of the wrist in Fig. 13 are verified to be larger than those in Fig. 14 because of the existence of large internal forces. The six-axis force/torque measurements in Type (b) are approximately 45% compared with the measurements in Type (a). It is clear from the experimental results that Type (b) can prevent the occurrence of large internal forces during the door-opening process.

During the experiments, it was noticed that there was less mutation of the six-axis force/torque measurements in using Type (b). This is because of the smaller relative motion generated between the robot end effector and the door handle using Type (b). The force in the z-direction F_{z2} in the handle-turning process and in the y-direction F_{y2} in the door-pulling process represents the main turning force and main pulling force, and they are expected to be large, mainly because of the force applied by the spring-loaded handle and spring-loaded door in these directions. The maximum torque measurements at the wrist were less than 50 Nm in the handle-turning process and less than 40 Nm in the door-pulling process.

The estimated values of the joints' torques are shown in Fig. 15, including Type (a) and Type (b). Comparing the estimated values of the joints' torques with different types explains the internal forces of each joint. From Fig. 15, the estimated values of the joints' torques using Type (a) are larger than

Table IV. Physical parameters of the experimental setup and control parameters.

Physical parameters					
Parameter	Value	Parameter	Value	Parameter	Value
Rotor inertia for joint 1	$I_{m1}=0.344\times10^{-4}(\mathrm{kg}\cdot\mathrm{m}^2)$	Rotor inertia for joint 3	$I_{m3}=0.216\times10^{-4}(\mathrm{kg}\cdot\mathrm{m}^2)$	Rotor inertia for joint 5	$I_{m5}=0.185\times10^{-4}(\mathrm{kg}\cdot\mathrm{m}^2)$
Link inertia for joint 1	$I_{l1}=\begin{bmatrix}0.0912 & 0 & 0\\ 0 & 0.08262 & 0.0027\\ 0 & 0.0027 & 0.0246\end{bmatrix}(\mathrm{kg}\cdot\mathrm{m}^2)$	Link inertia for joint 3	$I_{l3}=\begin{bmatrix}0.0166 & 0 & 0\\ 0 & 0.0062 & -0.0044\\ 0 & -0.0044 & 0.0144\end{bmatrix}(\mathrm{kg}\cdot\mathrm{m}^2)$	Link inertia for joint 5	$I_{l5}=\begin{bmatrix}0.0016 & 0 & 0\\ 0 & 0.0009 & 0.0005\\ 0 & 0.0005 & 0.0012\end{bmatrix}(\mathrm{kg}\cdot\mathrm{m}^2)$
Reduction for joint 1	$N_1=596$	Reduction for joint 3	$N_3=625$	Reduction for joint 5	$N_5=552$
Rotor inertia for joint 2	$I_{m2}=0.216\times10^{-4}(\mathrm{kg}\cdot\mathrm{m}^2)$	Rotor inertia for joint 4	$I_{m4}=0.185\times10^{-4}(\mathrm{kg}\cdot\mathrm{m}^2)$	Rotor inertia for joint 6	$I_{m6}=0.114\times10^{-4}(\mathrm{kg}\cdot\mathrm{m}^2)$
Link inertia for joint 2	$I_{l2}=\begin{bmatrix}0.0158 & 0 & 0.0093\\ 0 & 0.0860 & 0\\ 0.0093 & 0 & 0.0789\end{bmatrix}(\mathrm{kg}\cdot\mathrm{m}^2)$	Link inertia for joint 4	$I_{l4}=\begin{bmatrix}0.0049 & 0 & 0\\ 0 & 0.0032 & 0.0003\\ 0 & 0.0003 & 0.0034\end{bmatrix}(\mathrm{kg}\cdot\mathrm{m}^2)$	Link inertia for joint 6	$I_{l6}=\begin{bmatrix}0.0128 & 0 & 0.0002\\ 0 & 0.0129 & 0\\ 0.0002 & 0 & 0.0018\end{bmatrix}(\mathrm{kg}\cdot\mathrm{m}^2)$
Reduction for joint 2	$N_2=625$	Reduction for joint 4	$N_4=552$	Reduction for joint 6	$N_6=300$

Table V. Control parameters.

Control parameters			
Operational object parameters			
Parameter	Value	Parameter	Value
Maximum torque for handle	45 Nm	Maximum torque for door	35 Nm
Rotation radius for handle	76 mm	Rotation radius for door	850 mm
Internal torque estimation parameters			
Parameter	Value	Parameter	Value
Compliance model	$c_{\mathrm{f}i} = 0.089\,(\mathrm{N/m}) K_{\mathrm{f}i} = 8333\,(\mathrm{N \cdot m/rad})$ $c_{\omega i} = 83.5\,(\mathrm{N/m}) K_{\omega i} = 1.33\,(\mathrm{N \cdot m/rad})$	Kinematic error model	$a_{0i} = 0.001$, $a_{l1i} = -0.1476 \times 10^{-3}$, $b_{l1i} = -0.4309 \times 10^{-2}$, $\omega_{li} = 0.01731$, $a_{\omega 1i} = 0.1594 \times 10^{-2}$, $b_{\omega 1i} = -0.1819 \times 10^{-2}$, $a_{\omega 2i} = 0.3288 \times 10^{-2}$, $b_{\omega 2i} = 0.9049 \times 10^{-3}$, $\omega_{\omega i} = 0.01734$
Controller parameters			
Parameter	Value	Parameter	Value
Robust adaptive term	$\rho_{\mathrm{F}_1} = 0.12$, $\rho_{\mathrm{F}_2} = 0.08$, $\rho_{\mathrm{F}_{3-6}} = 0.04$ $\lambda_{\mathrm{i}} = 0.45$, $\rho_{base} = 0.8, \rho_{f_{m1}} = 0.14$, $\rho_{f_{m2}} = 0.12$, $\rho_{f_{m3-6}} = 0.02$ $\rho_{\tau_{ineri}} = 0.9, \varepsilon_{ri} = 0.01 \rho_{\mathrm{F}_{ij}} = 0.01, \varepsilon_{\mathrm{F}_{ij}} = 0.01$	Friction compensation	$\varepsilon_{\dot{q}_{mi}} = 0.001 \hat{b}_1^c = 0.013$, $\hat{b}_2^c = 0.008$, $\hat{b}_{3-6}^c = 0.002$ $\hat{f}_{c1}^c = 0.01$, $\hat{f}_{c2}^c = 0.008$, $\hat{f}_{c3-6}^c = 0.003$ $\hat{f}_{s1}^c = 0.002$, $\hat{f}_{s2}^c = 0.0015$, $\hat{f}_{s3-6}^c = 0.001$ $\hat{f}_{\tau 1}^c = 0.048$, $\hat{f}_{\tau 2}^c = 0.026$, $\hat{f}_{\tau 3-6}^c = 0.012$

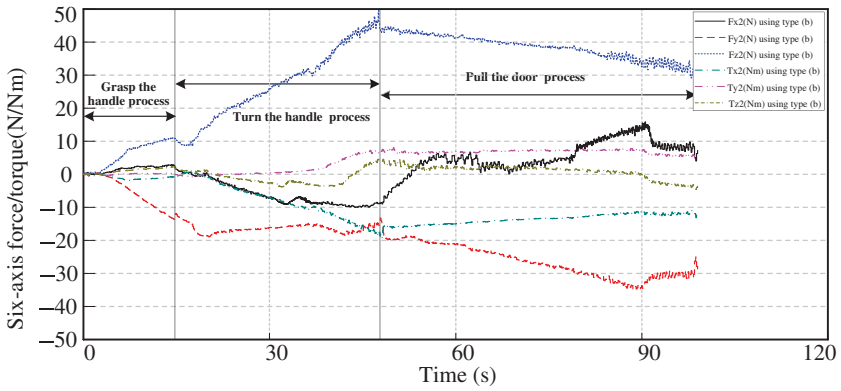

Fig. 14. Six-axis force/torque measurements of the wrist with Type (b).

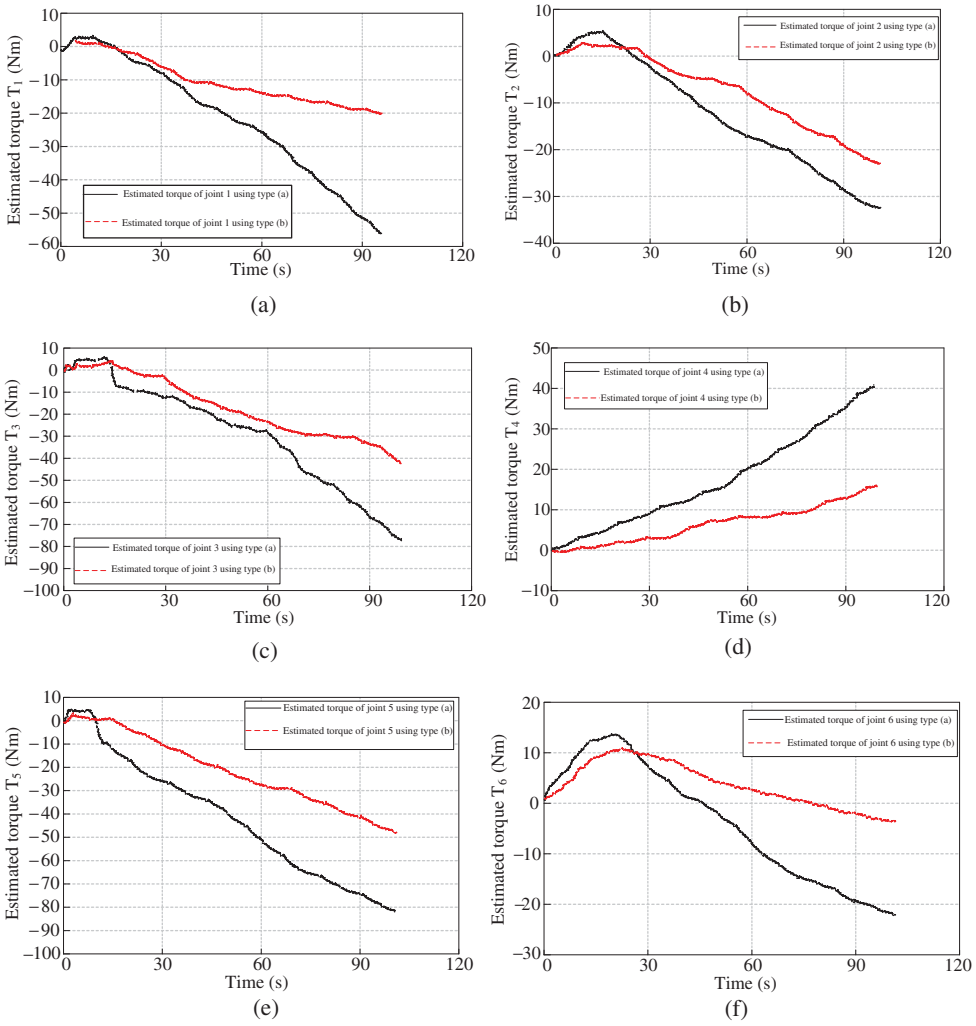

Fig. 15. Estimated torques of the joints. (a) Position and estimated torque of joint 1. (b) Position and estimated torque of joint 2. (c) Position and estimated torque of joint 3. (d) Position and estimated torque of joint 4. (e) Position and estimated torque of joint 5. (f) Position and estimated torque of joint 6.

those using Type (b); this shows that the internal forces using Type (a) are larger than those using Type (b).

6. Conclusions

A new method for opening doors by a mobile manipulator in a rescue environment was developed using an unknown-force-related constraints estimation approach and a robust adaptive control algorithm. The mobile base achieves compliance when it comes into contact with the handle, by using force/torque feedback-based control. Unlike the existing door-opening method for mobile manipulators, the unknown force-related constraints are estimated on the basis of manipulator joint position measurements instead of force/torque sensors that may be expensive or affected by computational delays and physical conditions (e.g., temperature, humidity, or radiation). The method also considers the entire process of a door-opening task, including searching for/reaching the door, grasping the door handle, turning the door handle, and pulling the door. The method can be extended to more complex tasks having similar constraints, such as manipulating a valve or butting a joint pipe.

However, a method is never a perfect solution to a robot's task process. Even so, this paper's contribution focuses on the development of a new method for opening doors by a mobile manipulator in a rescue environment that provides a better solution of the working process with force constraints. Two experiments were conducted to confirm the utility and validity of the proposed method. In the first one, a method proposed in the literature[30] was employed to describe the door-opening task whose controller requires only the joint planning positions. The second experiment involved the unknown-force-related constraints estimation approach that can be regarded as a robust adaptive control algorithm. Two types of experimental results demonstrated that the method proposed in this study can avoid the occurrence of large internal forces in the joints. This feature is highly important, especially in a rescue environment, because it is not necessary for the design of protected force/torque sensors are that can reduce the precision and increase the mass. The method proposed in this study supplies another option for similar robot tasks.

Acknowledgments

This work was supported by the National Key Basic Research Development Plan Project (973) (2013CB035502), National Natural Science Foundation of China (Grant No. 61370033/51275106), Harbin Talent Program for Distinguished Young Scholars (No. 2014RFYXJ001), Fundamental Research Funds for the Central Universities (Grant No. HIT.BRETIII.201411), Foundation of Chinese State Key Laboratory of Robotics and Systems (Grant No. SKLRS201401A01), Postdoctoral Youth Talent Foundation of Heilongjiang Province, China (Grant No. LBH-TZ0403), and the "111" Project (B07018).

References

1. S. Ahmad, H. Zhang and G. Liu, "Multiple working mode control of door-opening with a mobile modular and reconfigurable robot," *IEEE/ASME Trans*. **2**, 115–122 (2012).
2. R. Brooks, L. Aryananda, A. Edsinger, P. Fitzpatrick, C. Kemp, U. M., O'Reilly, E. Torres-Jara, P. Varshavskaya and J. Weber, "Sensing and manipulating built-for-human environments," *Int. J. Humanoid Robot.* **1**(1), 1–28 (2004).
3. W. Chung, C. Rhee, Y. Shim, H. Lee and S. Park, "Door-Opening control of a service robot using the multifingered robot hand," *IEEE Trans. Ind. Electron.* **56**(10), 3975–3984 (2009).
4. L. Ding, H. Gao, K. Xia, Z. Liu, J. Tao and Y. Liu, "Adaptive sliding mode control of mobile manipulators with Markovian switching joints," *J. Appl. Mathematics*, **10**(3), 812–836 (2012).
5. W. Huang, K. Tanie and S. Sugano, "Coordinated motion planning for a mobile manipulator considering stability and manipulation," *Int. J. Robot. Res.* **19**(8), 732–742 (2000).
6. F. Inoue and T. Murakami, "A motion control of mobile manipulator with external force," *IEEE/ASME Trans. Mechatronics*, **6**(2), 137–142 (2001).
7. R. Jamisola, M. Ang, D. Oetomo, O. Khatib, T. Lim and S. Lim, "The Operational Space Formulation Implementation to Aircraft Canopy Polishing using a Mobile Manipulator," *Proceedings of the IEEE International Conference on Robotics and Automation*, Washington. New York: IEEE Press, vol. 1 (2002) pp. 400–405.
8. S. Katsura, Y. Matsumoto and K. Ohnishi, "Modeling of force sensing and validation of disturbance observer for force control," *IEEE Trans. Ind. Electron.* **54**(1), 530–538 (2007).

9. O. Khatib, K. Yokoi, O. Brock, K. Chang and A. Casal, "Robots in human environment: Basic autonomous capabilities," *Int. J. Robot. Res.* **18**(7), 684–696 (1999).
10. D. Kim, J. Kang, C. Hwang and K. Park, "Mobile Robot for Door Opening in a House," **In**: *Knowledge-Based Intelligent Information and Engineering Systems*, Vol. **LNAI-3215** (Springer-Verlag, New York, 2004) (pp. 596–602).
11. E. Klingbeil, A. Saxena and A. Y. Ng, "Learning to Open New Doors," *AAAI 17th Annual Robot Workshop and Exhibition*, Chicago (2008) pp. 2751–2757.
12. S. Kobayashi, Y. Kobayashi, Y. Yamamoto, T. Watanabe, Y. Ohtsubo, T. Inoue, M. Yasuda and Y. Takamori, "Development of a Door Opening System on Rescue Robot for Search' UMRS-2007," *Proceedings of the SICE Annual Conference*, Tokyo. Tokyo: The Society of Instrument and Control Engineers (SICE) (2008) pp. 2062–2065.
13. D. Kragic, L. Petersson and H. I. Christenseni, "Visually guided manipulation tasks," *Robot. Autonomous Syst.* **40**(2), 193–203 (2002).
14. Z. Li, S. S. Ge, M. Adams and W. S. Wijesoma, "Adaptive robust output-feedback motion/force control of electrically driven nonholonomic mobile manipulators," *IEEE Trans. Control Syst. Technol.* **16**(6), 1308–1315 (2008a).
15. Z. Li, S. S. Ge, M. Adams and W. S. Wijesoma, "Robust adaptive control of uncertain force/motion constrained nonholonomic mobile manipulators," *Automatica*, **44**(3), 776–784 (2008b).
16. Z. Li, S. S. Ge and Z. Wang, "Robust adaptive control of coordinated multiple mobile manipulators," *Mechatronics*, **18**, 239–250 (2008).
17. G. Liu, "Decomposition-based friction compensation of mechanical systems," *Mechatronics*, **12**(5), 755–769 (2002).
18. G. Liu, A. A. Goldenberg and Y. Zhang, "Precise slow motion control of a direct-drive robot arm with velocity estimation and friction compensation," *Mechatronics*, **14**(7), 821–834 (2004).
19. K. Nagatani and S. Yuta, "Designing a Behavior to Open a Door and to Pass Through a Door-Way Using a Mobile Robot Equipped with a Manipulator," *Proceedings of the IEEE/RSJ International Conference on Intelligent Robots & Systems*, vol. 2, Munich, New York: IEEE Press, vol. 2 (1994) pp. 847–853.
20. K. Nagatani and S. I. Yuta, "An Experiment on Opening-Door-Behavior by an Autonomous Mobile Robot with a Manipulator," *Proceedings of the IEEE/RSJ International Conference on Intelligent Robots & Systems*, vol. 2, Pittsburgh. New York: IEEE Press, vol. 2 (1995) pp. 45–50.
21. K. Nagatani and S. Yuta, "Designing Strategy and Implementation of Mobile Manipulator Control System for Opening Door," *Proceedings of the IEEE International Conference on Robotics & Automation*, vol. 3, Minneapolis. New York: IEEE Press, vol. 3 (1996) pp. 2828–2834.
22. G. Niemeyer and J. J. E. Slotine, "A Simple Strategy for Opening an Unknown Door," *Proceedings of the IEEE International Conference on Robotics and Automation*, vol. 2, Albuquerque. New York: IEEE Press, vol. 2 (1997) pp. 1448–1453.
23. L. Petersson, D. Austin and D. Kragic, "High-Level Control of a Mobile Manipulator for Door Opening," *Proceedings of the IEEE/RSJ International Conference on Robots and Systems*, vol. 3, Takamatsu. New York: IEEE Press, vol. 3 (2000) pp. 2333–2338.
24. L. Petersson, D. Austin, D. Kragic and H. I. Christensen, "Towards an Intelligent Service Robot System," *Proceedings of the International Conference on Intelligent Autonomous Systems*, Venice (2000) pp. 704–709.
25. K. Xia, L. Ding, H. Gao, Z. Deng, G. Liu and Y. Wu, "Switch Control for Operating Constrained Mechanisms Using a Rescuing Mobile Manipulator with Multiple Working Modes," *IEEE International Conference on Advanced Robotics and Mechatronics (ICARM)*, (Oct. 2016) (pp. 139–146).
26. B. J. W. Waarsing, M. Nuttin and H. van Brussel, "Behaviour-based Mobile Manipulation: The Opening of a Door," *Proceedings of the 1st International Workshop on Advanced Serv. Robot.*, Bardolino (2003) pp. 168–175.
27. H. Zhang, S. Ahmad and G. Liu, "Torque estimation for robotic joint with harmonic drive transmission based on position measurements," *IEEE Trans. Robot.* **31**(2), 322–330 (2015).
28. K. Xia, H. Gao, L. Ding, G. Liu, Z. Deng, Z. Liu and C. Ma, "Trajectory Tracking Control of Wheeled Mobile Manipulator Based on Fuzzy Neural Network and Extended Kalman Filtering," **In**: *Neural Computing and Applications* (2016) pp. 1–16.